https://doi.org/10.5194/wes-2021-142
Preprint. Discussion started: 20 January 2022

eawe european academy of wind energy
Open Access WIND ENERGY SCIENCE DISCUSSIONS

Effect of different source terms in atmospheric boundary modelling over the complex terrain site of Perdigao

Kartik Venkatraman[1,2,*], Trond-Ola Hågbo[1,3,*], Sophia Buckingham[1], and Knut Erik Teigen Giljarhus[3]

[1]von Karman Institute for Fluid Dynamics, Waterloosesteenweg 72, B-1640 Sint-Genesius-Rode, Belgium
[2]Université de Sherbrooke, Canada
[3]University of Stavanger, Norway
[*]These authors contributed equally to this work.

Correspondence: kartik.venkatraman@vki.ac.be

Abstract. The assessment of wind conditions in complex terrain requires the use of Computational Fluid Dynamics (CFD) simulations incorporating an accurate parameterization of forest canopy effects and variable thermal stability effects. This study aims to investigate how incorporating the presence of trees can improve the flow predictions. A three-dimensional steady Reynolds-averaged Navier-Stokes (RANS) equations model is set up using OpenFOAM to simulate the flow over a complex terrain site comprising two parallel ridges located near Perdigão, Portugal. A 7.5 km $\times$ 7.5 km terrain of the Perdigao site is constructed from elevation data centered around a 100 m met-mast located on the northeast ridge. A 30-min averaged stationary period corresponding to near-neutral conditions on a single met-mast tower is simulated. The impact of incorporating different source terms is studied such as forest canopy, Coriolis forces as well as also buoyancy forces. The prediction capability of the models is analyzed for different groups of towers on the South-West ridge, inside the valley and on the North-East ridge based on the flow topology. The inclusion of a canopy model is shown to improve predictions close to the ground for most of the towers, while reducing prediction accuracy on top of the ridges, illustrating the need to represent terrain heterogeneity.

1 Introduction

Lack of terrain availability in flat terrain pushes wind-farm developers to look for alternative sites along complex terrains. Flat terrain availability is becoming scarce and 70% of the Earth's surface is in complex terrain, which presents large potential for wind energy harvesting. Winds in complex terrains are governed by the surface properties of the flow (land class/roughness) and the local elevation such as hills, ridges and mountains (Emeis, 2018). Local features such as ridges or canyons can also be advantageous for wind energy harvesting, due to the creation of local flow accelerations on top of ridges and flow channeling through valleys. However, the wind fields are dependent on either the local pressure or temperature gradient. Such flows are also dominated by strong thermal stratification effects and are influenced by presence of forest canopies. Complex terrains remain very challenging areas to consider for wind farm siting and require extensive validation of modeling tools in representative environments. Wind farm modeling for complex terrains requires a more advanced approach than commonly used cost-effective linearized models such as WAsP (Jørgensen et al., 2005) which cannot handle complex phenomena (i.e. flow separation) to ensure reliable and accurate results. Computational fluid dynamics (CFD) tools are increasingly used to predict

https://doi.org/10.5194/wes-2021-142
Preprint. Discussion started: 20 January 2022

eawe european academy of wind energy
Open Access WIND ENERGY SCIENCE DISCUSSIONS

flows over complex terrains to account for such phenomena and provide more reliable wind resource predictions (Blocken, 2014). However, improving numerical modeling tools for complex terrains demands accounting for various microscale phenomena such as flow re-circulation and the forest canopy effect. Such microscale flow features have a significant impact on local wind resource assessment and wind turbine loading.

Inital studies in literature accounting for effects of forest canopy were performed over forested flat terrains. Brower (2012) showed that the presence of a forest canopy increases the modelling uncertainty by up to a factor of 5 irrespective of the chosen modelling approach. Finnigan (2000) parameterized the effect of foliage and forest canopy by accounting for the drag force in the momentum equation. The effect of canopy on turbulence was further taken into account by Sogachev and Panfyorov (2006) and Sogachev (2009) by adding additional source terms for turbulence kinetic energy and turbulence dissipation rate. Desmond et al. (2017) modelled both forest canopy and buoyancy effects by modelling them using source and sink terms and showed that the thermal stratification plays an important role in determining the flow over canopies. The canopy model is typically implemented by specifying the tree height and leaf area density (LAD), which represents the area of the leaf and branches of trees. These parameters are typically defined from field measurements or LiDAR point clouds generated from field measurement campaigns and aerial surveys (Queck et al., 2012).

Validation of numerical models for complex terrains requires field measurements. One of the earliest field campaigns was at Askervin hill (Salmon et al., 1988), which is a smooth isolated hill. Similarly, the Bolund hill campaign was another campaign over an isolated hill in Denmark (Bechmann et al., 2009) with data under conditions which could be classified as neutral. However no canopy is seen on these sites. The Alaiz field campaign (Rodrigo et al., 2021) was performed over a large scale homogeneous mountain valley topography in Spain with forested regions. Chavez et al. (2014) showed that using a canopy model improved the accuracy of velocity and turbulence predictions for simulations over Alaiz.

More recently, a field experiment campaign has been carried out over the complex terrain terrain site at Perdigão, Portugal ((Fernando et al., 2018)) which is a double ridge with forested canopy experiencing different thermal stratification conditions. Significant field data is available for further studies and is further elaborated in Section 2. Several numerical studies have been performed for validation with field data. Laginha Palma et al. (2020) studied the choice of using the appropriate grid size for numerical modelling. Wagner et al. (2019) implemented a forest parameterization in the Weather Research and Forecasting model (WRF) with an average tree height of 30 m, resulting in an improvement in prediction of near surface wind speeds. This was chosen due to practical reasons related to the model setup and is not representative of actual tree height. There is a gap in existing literature on microscale simulations using a canopy model on a heterogeneous forested complex terrain with a rich dataset such as Perdigão. This study aims to address that research gap by investigation of the effect of specific microscale effects related to the modeling of trees and buoyancy effects at the complex terrain test-case of Perdigão at several met-mast locations and to verify if the forest parameterization helps improve predictions using a RANS simulation approach.

1.1 Objectives and outline

This paper aims to evaluate the impact of different physical source terms and turbulence models when performing CFD simulations in complex terrain and compare simulation prediction with field measurement profiles at the different groups of towers

https://doi.org/10.5194/wes-2021-142
Preprint. Discussion started: 20 January 2022

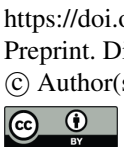

eawe european academy of wind energy
Open Access WIND ENERGY SCIENCE DISCUSSIONS

located at the Perdigão test site. The influence of the following parameters are investigated: Canopy effects, Coriolis force, impact of non-neutral effects (buoyancy forces).

An improved understanding of the importance of these phenomena will enable development of more efficient and reliable tools to perform wind simulations in complex terrain. This paper is structured as follows: a detailed description of the methodology is provided in Section 2, covering the computational domain and meshing, the numerical settings and different modeling capabilities that have been added as source terms to the conservation equations. The results are presented and discussed in Section 3, in terms of different groups of towers. Section 4 is dedicated to concluding remarks and future perspectives.

2 Perdigão Field measurement campaign

An intensive observation period was carried out from 1 May 2017 to 15 June 2017 at the double ridge site of Perdigão, Portugal by a consortium of American & European universities (Fernando et al. 2018). The location of the different met masts of heights 60 m and 100 m is shown in Fig. 2, which could be grouped by their location on top of the South-West ridge, inside the valley, or at top of the North-East ridge. From the analysis of the wind rose, the predominant directions at Tower 20 and Tower 29 are perpendicular to the ridges, i.e North-East and South-West directions, as shown in Fig 1, while at Tower 25, flow turning is seen and the dominant wind direction is from the South.

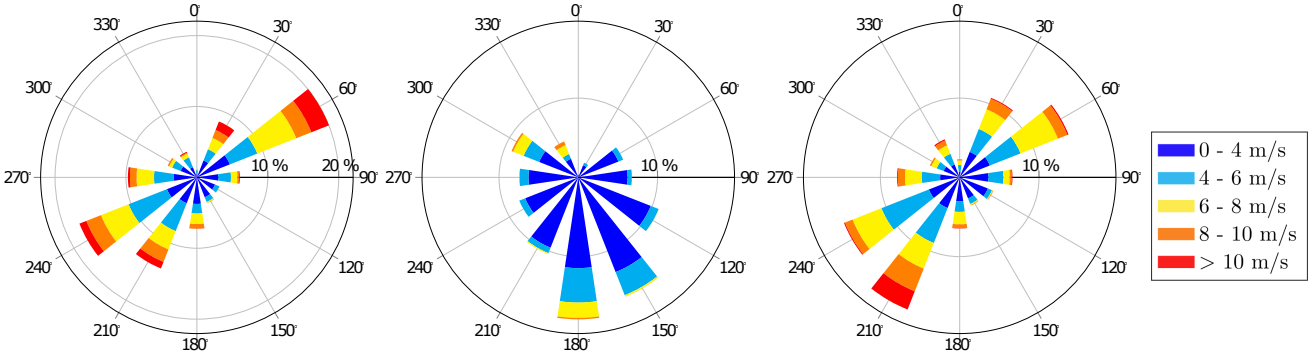

(a) Tower 20 (tse04). (b) Tower 25 (tse09). (c) Tower 29 (tse13).

Figure 1. Wind rose for 1 month period of May 2017 for towers on top of the ridges and inside the valley.

https://doi.org/10.5194/wes-2021-142
Preprint. Discussion started: 20 January 2022

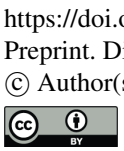

eawe european academy of wind energy
Open Access WIND ENERGY SCIENCE DISCUSSIONS

Figure 2. Elevation map and locations of interest at Perdigao. Positions of the measurements towers in the SW ridge group are indicated with + symbols, likewise are NE masts marked with x, and the masts in the inside valley group are indicated with black dots. The blue dots and the line represents the flow visualization slice used in Fig. 13. PT-TM06/ETRS89 coordinate system, height above sea level.

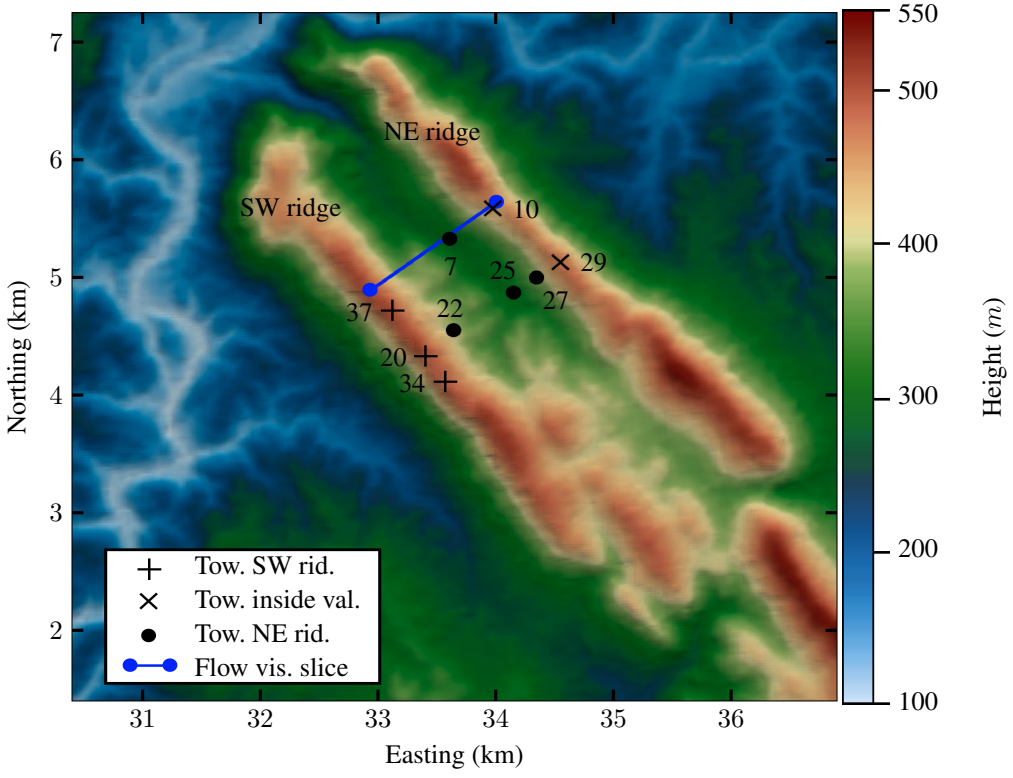

A stationary period was found on the date of 4th May, 2017 for the 30 minute averaged time interval of $22:00-22:30$ tilt corrected high frequency dataset from NCAR-EOL, based on the conditions at Tower 20 on top of the ridge, which corresponded to a bulk Richardson number of approximately -0.03 which qualifies as near-neutral condition. The bulk Richardson number (Kaimal and Finnigan, 1994) is calculated using Eqn 1. However, the flow conditions are non-neutral at other met mast locations.

$$Ri_b = \frac{g(\bar{\theta_{100}} - \bar{\theta_2})\Delta z}{\bar{\theta_{100}}[U_{100}^2 + V_{100}^2]} \tag{1}$$

where θ is the potential temperature, g is the acceleration due to gravity, U, V are the wind velocity components at the reference height (m). The same period was simulated by Laginha Palma et al. (2020) based on the stationary periods predicted by Carvalho (2019).

https://doi.org/10.5194/wes-2021-142
Preprint. Discussion started: 20 January 2022

eawe european academy of wind energy
Open Access WIND ENERGY SCIENCE DISCUSSIONS

3 Methodology

The terrain is a $7.5\,\mathrm{km} \times 7.5\,\mathrm{km}$ square centralized around a $100\,\mathrm{m}$ met-mast located on the south-west ridge. Fig 3 presents the computational domain and the dimensions are listed on the right side of the figure.

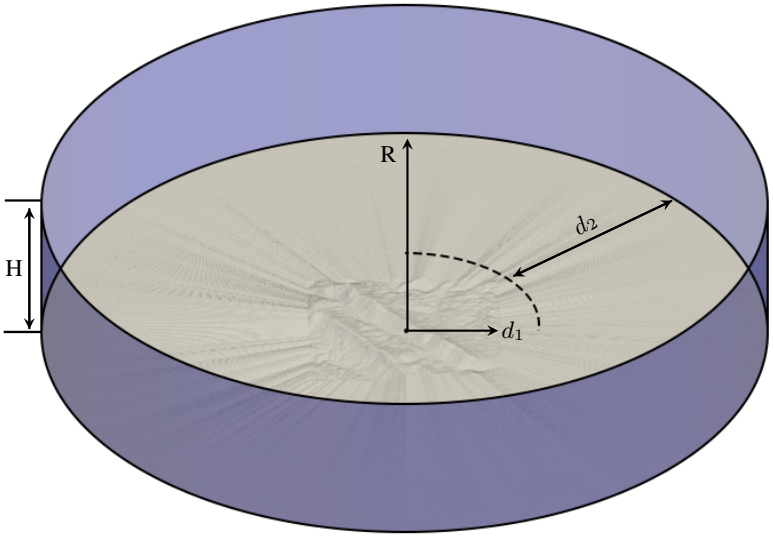

Figure 3. Computational domain, Δh_t is the difference in the elevation height of the terrain.

A cylindrical computation domain was developed, which provides the flexibility to simulate wind from any wind direction. This approach has also been successfully applied by the authors in a previous study pertaining to urban areas (Hågbo et al. 2020). A smoothing region from complex to flat terrain was applied towards the outer boundaries, with a minimum radial distance of 15 Δh_t. Several best practice guidelines have been formulated for grid generation for simulating complex terrains, such as by Sørensen et al. (2012) and Laginha Palma et al. (2020) and have been closely followed. The height of the domain is set to ten times the difference in the elevation height of the terrain, Δh_t, as recommended by Sørensen et al. (2012) when simulating wind flow over complex terrains. It consists of 12.7 million cells and is produced with `terrainBlockMesher` (Schmidt et al., 2012), capable of generating structured meshes over complex terrain exclusively consisting of hexahedra cells. Terrestrial data was obtained from the Shuttle Radar Topography Mission (SRTM) database of the Perdigão field experiment (Fernando et al., 2018). The horizontal mesh resolution over the terrain was set to $33\,\mathrm{m}$. It satisfies the minimum resolution of $40\,\mathrm{m}$ recommended specifically for the Perdigão site by Laginha Palma et al. (2020). A uniform stretching is applied in the vertical direction. A mesh sensitivity study was performed to ensure that the grid resolution is sufficiently high and for the predictions in the area of interest no significant changes were observed. Fig 4 illustrates the grid structure used inside the domain from the side. The mesh also follows the recommendation for having at least three cells from the ground to the height at the first sampling point for comparison with field measurements.

https://doi.org/10.5194/wes-2021-142
Preprint. Discussion started: 20 January 2022

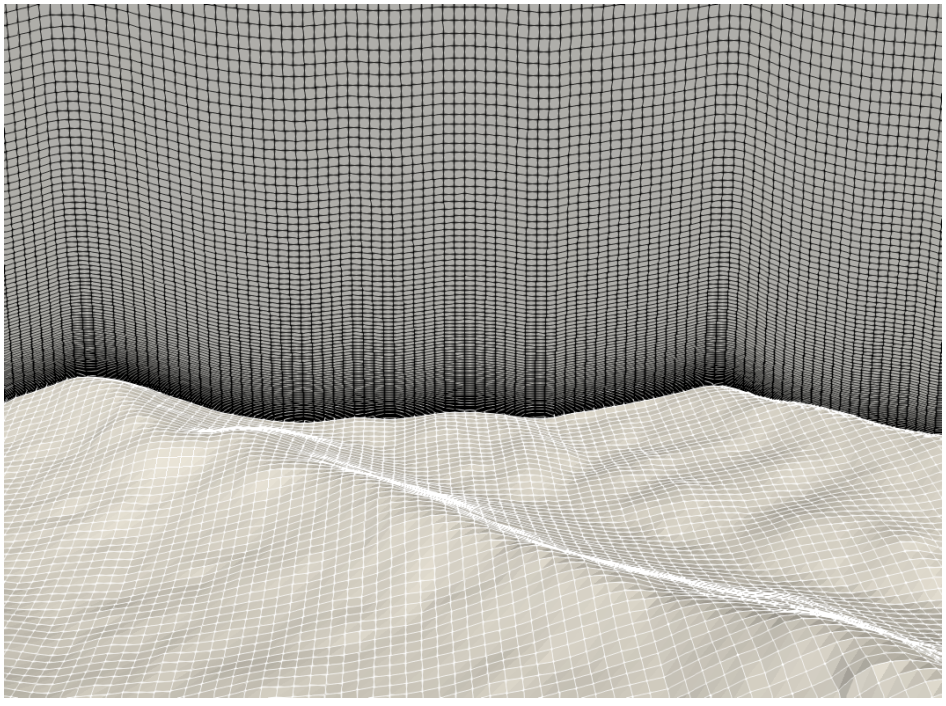

Figure 4. Computational grid structure, partial view from the side.

All simulations have been conducted using the OpenFOAM (version 2012) toolbox. The simulations are steady-state and performed by solving the incompressible, three-dimensional steady Reynolds-averaged Navier-Stokes (RANS) equations with the finite volume method. Second-order discretization schemes were used for the spatial discretization. The initial iterative convergence criteria were that the scaled residuals should drop four orders of magnitude for all flow variables as per the BPGs. Two steady-state solvers for turbulent flow of incompressible fluids have been used: `simpleFoam` (SF) and `buoyantBoussinesqSimpleFoam` (BBSF). All thermal effects are neglected in the simulations using the SF solver, such that the atmospheric stability of the simulated atmosphere is always neutral. In these simulations, the air density is assumed constant, and the gravitational force is neglected. The effect of buoyancy forces is included in the simulations using the BBSF solver. In addition to solving the continuity equation and the momentum equation, which is solved using SF, the energy equation is solved. It allows for the modeling of non-neutral atmospheric conditions. The solver uses the Boussinesq approximation, which ignores density differences except where they appear in terms multiplied by the gravitational acceleration.

3.1 Inlet profiles and Boundary conditions

Two sets of fixed inlet profiles have been used, both forming a homogeneous atmospheric boundary layer (ABL). either idealized with a logarithmic velocity profile or fully developed profiles obtained from a precursor simulation. The precursor model is further described by Alletto et al. (2018) and Koblitz (2013).

https://doi.org/10.5194/wes-2021-142
Preprint. Discussion started: 20 January 2022

eawe european academy of wind energy
Open Access WIND ENERGY SCIENCE DISCUSSIONS

The idealized profiles provide the turbulence quantities and a log-law type ground-normal wind velocity based on the generalization and modification of the well-used set of equations from Richards and Hoaxey (1993). This modification has been implemented by Yang et al. (2009) and uses a more mathematically consistent formulation allowing the turbulent kinetic energy to vary with height. Also, using a log-low wind velocity profile and the associated turbulent inflow conditions are considered only to be valid in the atmospheric surface layer, which can be roughly estimated as 10% of the atmospheric boundary layer (Temel et al. 2018).

An alternative to using the idealized profiles is using fully developed profiles obtained from a one-dimensional precursor simulation following the strategies of Koblitz (2013), Alletto et al.(2018). Cyclic conditions are applied on the sides, and the simulations are run for sufficient iterations to allow development of the profile. The setups are identical to the setups used in the final (successor) simulations except for the computational domain and mesh, the cyclic conditions applied, and the number of iterations. It ensures consistent profiles. The effect of atmospheric stability, a tree canopy, the Coriolis frequency, and other parameters are modeled through source terms explained in the following section. It enables the precursor simulations to produce inlet profiles valid for various conditions, including non-neutral atmospheric conditions. Adjusting the parameters of these source terms is an efficient way to obtain the desired inflow. An overview of the boundary conditions (BCs) used is presented in Table 1.

Table 1. Overview of boundary conditions applied in the neutral simulation setup.

Patch	**Boundary condition type**
Sides	Inlet/outlet
Inlet	Fixed value profiles of an atmospheric boundary layer
Outlet	Zero gradient, and fixed pressure or fixed $(p-(\rho g h))$
Terrain	Rough wall, $z_0 = 0.02\,\mathrm{m}$
Top	Slip

Robin boundary conditions that act as an inlet or outlet are used on the sides of the domain to simulate wind from any direction. The direction of the flux automatically determines the inlet and outlet regions. The inlet profiles are fixed to form a homogeneous atmospheric boundary layer (ABL), either idealized profiles representing neutral atmospheric conditions or fully developed profiles obtained from precursor simulation (van der Laan et al., 2020). At the outlet, outlet conditions were used with constant pressure in the simulations using the SF solver, or equally, constant $(p-(\rho g h))$ in the simulations using the BBSF solver. Zero gradient was set for the remaining variables. The direction of the flux automatically determines the inlet and outlet regions. No-slip conditions with wall functions were used for the terrain. Specifically, a rough wall condition was applied (Hargreaves and Wright, 2007). The roughness was set to $z_0 = 0.02\,\mathrm{m}$, based on average values of a roughness map provided at the database of the Perdigão field experiment (Fernando et al., 2018).

https://doi.org/10.5194/wes-2021-142
Preprint. Discussion started: 20 January 2022

eawe european academy of wind energy
Open Access WIND ENERGY SCIENCE DISCUSSIONS

3.2 Source terms

Four different source terms have been added to some of the simulation cases: Tree canopy as a porous medium, Coriolis force, Pressure gradient force, Buoyancy forces, maximum mixing length scale limiter for the mixing length turbulence model.

Some simulation cases include the modeling of a tree canopy through a source term. The canopy is modeled as a porous medium based on the work of Costa (2007). A drag term is added to the momentum equation and additional source terms for the production and dissipation of turbulence. The porous media is implemented through the power law porosity model. The parameters for the canopy modeling are the leaf area density, which is set to $0.14\,\mathrm{m}^{-1}$, and the drag coefficient of the trees, set to 0.25. A mean tree height of $3\,\mathrm{m}$ is chosen based on the mean canopy height at different locations provided by Vasiljevic et al. (2017). An overall tree height of $3\,\mathrm{m}$ is also supported by analyzing a LiDAR point cloud acquired from the database of the Perdigão field experiment (Fernando et al., 2018) as shown in Fig 5. The source term in the canopy model for velocity is as shown below:

$$S_p - = \alpha\rho\left(C_d LAD\,|u_o|\right)u \tag{2}$$

where LAD is the Leaf area density, C_d is the plant canopy drag coefficient.

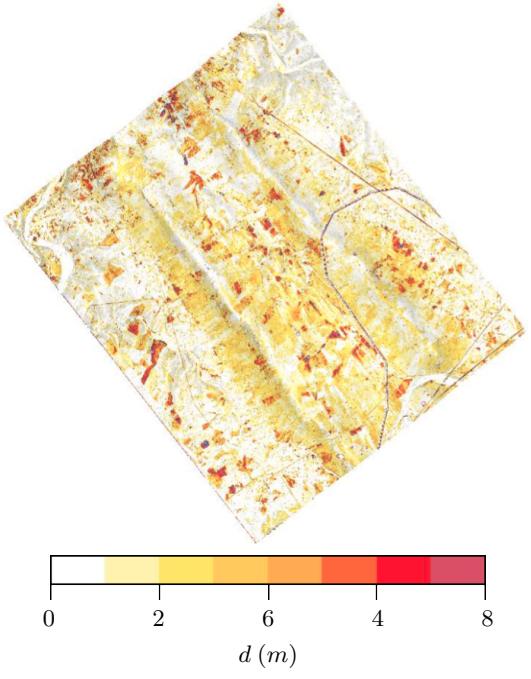

Figure 5. Minimum Euclidean distance, d, from the trees/vegetation to the bare ground effectively showing their height. Results obtained from analyzing a LiDAR point cloud acquired from the database of the Perdigao Field Experiment website *https://perdigao.fe.up.pt/*

https://doi.org/10.5194/wes-2021-142
Preprint. Discussion started: 20 January 2022

The magnitude and direction of the Coriolis force source term is calculated based on Earths' rotation and the Coriolis frequency parameter corresponding to the latitude of Perdigão shown in Eq. 3.

$$f_M - = \rho((2\Omega) \times u) \tag{3}$$

where Ω is the rotational period and ρ is the air density.

A pressure gradient force is also included in the simulation cases using the BBSF solver. In setups using this solver, the wind is driven by the balance of the lateral pressure gradient force and the Coriolis force. This balance is called geostrophic balance, and the resulting wind is a geostrophic wind, which in the Northern Hemisphere goes counterclockwise around low-pressure systems.

The inclusion of buoyancy forces is enabled by adding a heat/cooling flux on the terrain patch and adjusting the maximum mixing length scale, L_{max}, through the use of the source terms for turbulent kinetic energy and dissipation shown in Eqn. 4. These buoyancy forces are required in modeling non-neutral atmospheric effects and are only possible using the BBSF solver of the two solvers used .

$$B = \beta_B \alpha_{t_o} (\nabla T_o \cdot \boldsymbol{g}), \qquad S_p = \rho \frac{B}{k_o} k, \qquad S_p = \rho \frac{C_3 B}{k_o} \epsilon \tag{4}$$

where B is the buoyancy production term, β_B is the thermal expansion coefficient, α_{t_o} is the kinematic turbulent thermal conductivity, k is the turbulent kinetic energy, ϵ is the turbulent kinetic energy dissipation rate, C_3 is a model constant. Terms with the subscript denote values for previous iteration.

The level of turbulent kinetic energy is controlled in the domain by the use of a parameter called the maximum turbulent mixing length scale, used is to limit the production and dissipation terms of the turbulence model. The maximum global turbulent mixing length scale for a neutral ABL as is shown in Eq. 5 proposed by (Blackadar, 1962) and also used by (Koblitz, 2013).

$$L_o = 0.00027 \frac{G}{f_c} \tag{5}$$

where G is the geostrophic wind and f_c is the Coriolis frequency parameter.

3.3 Simulation cases

The setup for all the simulations was identical except for certain parameters. The solver used is either `simpleFoam` (SF) or `buoyantBoussinesqSimpleFoam` (BBSF). The inlet profiles, either idealized with a logarithmic velocity profile representing neutral atmospheric conditions or fully developed profiles obtained from precursor simulation. Source terms added, including canopy (tree height set to $3\,\mathrm{m}$) and the Coriolis force. Three turbulence models have been used: the standard k-ϵ turbulence model (SKE), a modified k-ϵ turbulence model (MKE), and the k-ω turbulence model (KO). The MKE model is applied in the simulation case where trees/vegetation (canopy) has been added as a porous medium with the SF solver. This

https://doi.org/10.5194/wes-2021-142
Preprint. Discussion started: 20 January 2022

model was tuned using experimental data and LES (Large Eddy Simulation) for a homogeneous forest (Costa 2007). With regards to the boundary conditions, they are overall the same but had to be adjusted to account for the different solvers and inlet profiles used. An overview of all the simulation cases is provided in Table 2.

Table 2. List of simulation cases simulating a period of neutral atmosphere, 22:00-22:30 (04.05.17).

Case name	**Solver**	**Inlet profiles**	**Source terms**				**Turbulence mod.**
			Canopy	Coriolis	Pres. gr.	Buoy. for.	
SF1	SF	Log-law	No	No	No	No	SKE
SF2	— " —	—— " ——	— " —	— " —	— " —	— " —	KO
SF3	— " —	—— " ——	Yes	— " —	— " —	— " —	MKE
SF4	— " —	—— " ——	No	Yes	— " —	— " —	SKE
BBSF1	BBSF	Precursor	— " —	— " —	Yes	Yes	——— " ———

4 Results

The results are discussed based on three groups of towers of interest: on top of the South-West ridge, inside the valley and on top of the North-East ridge. The inlet profiles for all the simulations are calibrated to match the measured velocity magnitude and direction at 100 m at tower 20, which corresponds to an elevation of 573 m. Different metrics are analyzed for all the simulation models at different towers and are further explained. The root mean square error (RMSE) between the averaged profiles of the measured data and the simulated results is computed and presented in Table 3. A hit rate metric for a given model is defined as the number of predictions predictions within one standard deviation over each height of the field measurement. The relative error for the turbulent kinetic energy and wind direction is shown in Tables 4, 5 respectively. The relative error is defined as the percentage of difference between the simulated and field measurement, which is divided by field measurement value.

4.1 Model prediction on SW ridge

The towers on the SW ridge as shown in Fig. 2 are the Tower 20, 34 and 37. This is a region of flow acceleration. A good match is obtained in between the measured and computed velocity, turbulent kinetic energy and wind direction profiles for the calibration Tower 20 as seen in Fig. 6. For Tower 34 shown in Fig 7 and for Tower 37 shown in Fig 8, the model including the canopy provides the best match. In models that do not account for a canopy, a speed up is seen close to the ground with large RMSE errors as seen in Table 3. The canopy model on the other hand predicts the shape of the profile correctly, but over predicts the turbulent kinetic energy for all the towers on the SW ridge. The results suggest that the inclusion of the canopy is a good choice for prediction of velocity profiles, however the parameter choice needs to be better optimised to reduce the levels of turbulence produced due by the canopy. In terms of the turbulence model, the $k-\epsilon$ model is seen to produce a slightly

https://doi.org/10.5194/wes-2021-142
Preprint. Discussion started: 20 January 2022

eawe european academy of wind energy
Open Access WIND ENERGY SCIENCE DISCUSSIONS

Table 3. RMSE for wind speed predictions on the main towers of interest

Case	Weather mast group	RMSE (m/s) Height over terrain							Average RMSE (m/s)	Hit rate (max 7)
		10 m	20 m	30 m	40 m	60 m	80 m	100 m		
SF1 (k-ϵ)	Tower 20	0.82	0.29	0.25	0.22	0.30	0.21	0.23	0.33	6
	Tower 25	0.90	1.05	1.02	0.84	0.73	0.59	0.57	0.81	3
	Tower 29	1.53	0.73	0.46	0.15	0.44	0.41	0.43	0.59	6
SF2 (k-ω)	Tower 20	0.78	0.23	0.20	0.17	0.26	0.17	0.19	0.29	6
	Tower 25	0.19	0.65	0.74	0.69	0.75	0.69	0.71	0.63	0
	Tower 29	0.66	0.96	1.19	1.19	1.37	1.28	1.23	1.12	1
SF3 (Canopy)	Tower 20	0.66	0.51	0.42	0.34	0.38	0.26	0.19	0.39	2
	Tower 25	0.18	0.39	0.42	0.45	0.63	0.84	1.02	0.56	0
	Tower 29	2.40	3.03	3.20	3.16	3.17	2.99	2.81	2.97	0
SF4 (Coriolis)	Tower 20	0.41	0.57	0.59	0.62	0.88	0.82	0.85	0.68	6
	Tower 25	1.52	1.84	1.84	1.69	1.52	1.24	1.11	1.54	3
	Tower 29	0.65	1.47	1.76	1.88	2.08	1.87	1.75	1.64	0
BBSF1 (Buoyancy)	Tower 20	1.02	0.42	0.38	0.33	0.08	0.09	0.09	0.34	6
	Tower 25	1.52	1.73	1.81	1.79	1.94	2.13	2.28	1.89	0
	Tower 29	2.08	1.26	0.95	0.70	0.39	0.42	0.48	0.89	5

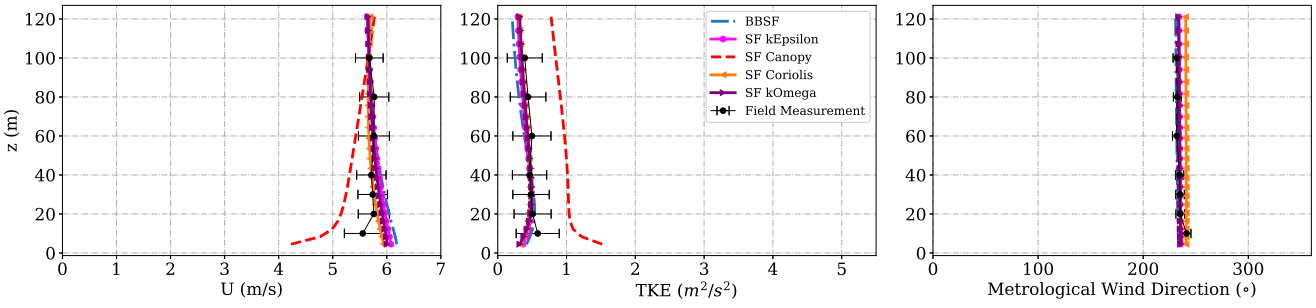

Figure 6. Simulation results and experimental data in tower 20/ tse04 for SW winds: (a) wind speed, (b) turbulent kinetic energy (c) wind direction

greater speed up compared to the $k-\omega$ model, but overall the prediction capability for the wind speed, turbulent kinetic energy and wind speed is similar.

https://doi.org/10.5194/wes-2021-142
Preprint. Discussion started: 20 January 2022

eawe european academy of wind energy
Open Access WIND ENERGY SCIENCE DISCUSSIONS

Table 4. Relative error and hit rate metrics for turbulent kinetic energy predictions at the main towers of interest

Case	Weather mast group	Average relative difference in TKE %	Hit rate (max 7)
SF1 (k-ϵ)	Tower 20	11.27	7
	Tower 25	55.43	6
	Tower 29	46.02	4
SF2 (k-ω)	Tower 20	9.93	7
	Tower 25	59.20	4
	Tower 29	24.26	5
SF3 (Canopy)	Tower 20	105.65	0
	Tower 25	61.40	3
	Tower 29	34.26	4
SF4 (Coriolis)	Tower 20	10.65	7
	Tower 25	55.77	6
	Tower 29	42.52	3
BBSF1 (Buoyancy)	Tower 20	16.80	7
	Tower 25	35.71	7
	Tower 29	57.66	0

Table 5. Relative error and hit rate metrics for wind direction predictions at the main towers of interest

Case	Weather mast group	Average difference in wind direction %	Hit rate (max 7)
SF1 (k-ϵ)	Tower 20	1.99	6
	Tower 25	36.59	4
	Tower 29	4.18	7
SF2 (k-ω)	Tower 20	1.84	6
	Tower 25	53.23	2
	Tower 29	4.22	7
SF3 (Canopy)	Tower 20	1.82	6
	Tower 25	74.43	0
	Tower 29	7.00	4
SF4 (Coriolis)	Tower 20	6.25	6
	Tower 25	135.81	2
	Tower 29	11.82	7
BBSF1 (Buoyancy)	Tower 20	2.39	6
	Tower 25	28.26	7
	Tower 29	5.34	7

https://doi.org/10.5194/wes-2021-142
Preprint. Discussion started: 20 January 2022

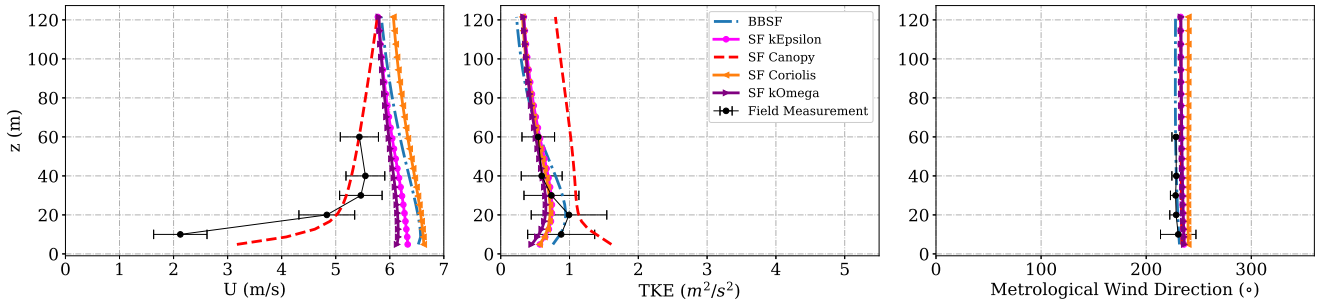

Figure 7. Simulation results and experimental data in tower 34/ rsw03 for SW winds: (a) wind speed, (b) turbulent kinetic energy (c) wind direction

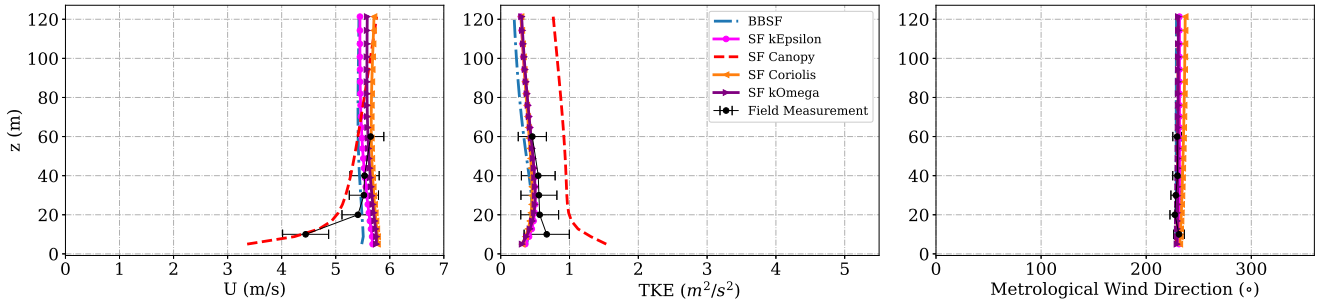

Figure 8. Simulation results and experimental data in tower 37/ rsw06 for SW winds: (a) wind speed, (b) turbulent kinetic energy (c) wind direction

4.2 Model prediction inside the valley

The towers of interest inside the valley are Towers 25, 22, 27 and 7. The predicted velocity, turbulent kinetic energy and wind direction profiles are shown in Figs 9, 10 and 12 respectively. This is a region of strong flow separation and flow re-circulation. The measured values of turbulent kinetic energy is high inside the valley, indicative of flow mixing and high turbulence, however all the models seem to strongly under predict the turbulent kinetic energy with large relative errors as seen in Table 4, except for Tower 22 which is the closest to the South-West ridge. Almost all models seen to provide a good prediction of the velocity profiles and TKE at that location, however a sudden shift in wind direction, indicative of a flow separation and re-circulation is seen in Fig 11. The buoyancy model provides a good hit rate for the wind direction inside the valley as shown in Table 5. On comparison of the turbulence the turbulence model, the $k-\epsilon$ model performs better than the $k-\omega$ model in prediction of wind velocity. Fig. 13 shows the velocity contour for the predicted re-circulation zone inside the valley using the canopy and buoyancy models. The model with the canopy produces a larger re-circulation zone compared to the other models.

https://doi.org/10.5194/wes-2021-142
Preprint. Discussion started: 20 January 2022

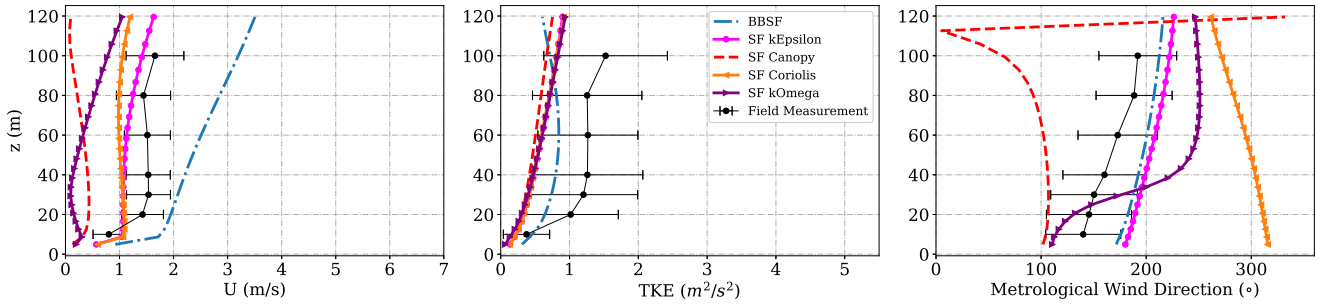

Figure 9. Simulation results and experimental data in tower 25/ tse09 for SW winds: (a) wind speed, (b) turbulent kinetic energy (c) wind direction

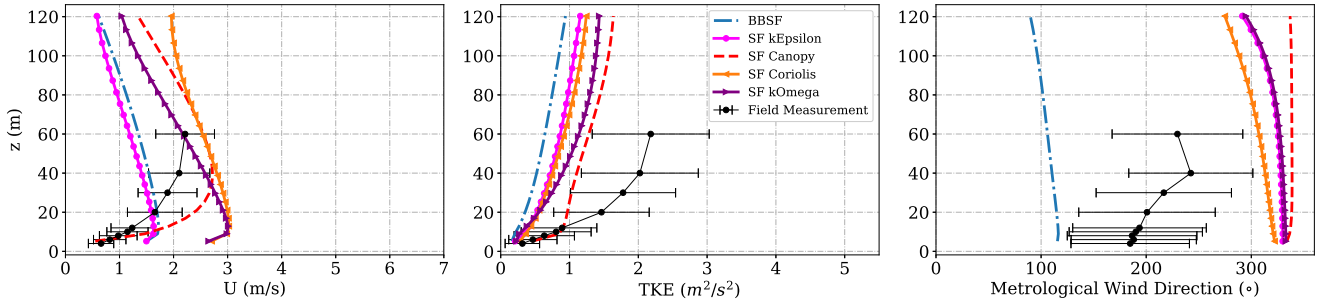

Figure 10. Simulation results and experimental data in tower 7/ tnw07 for SW winds: (a) wind speed, (b) turbulent kinetic energy (c) wind direction

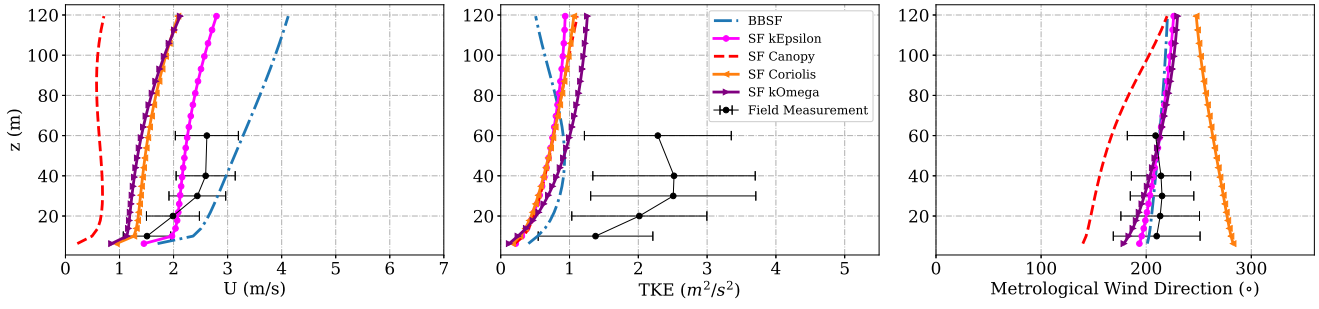

Figure 11. Simulation results and experimental data in tower 27/ tse11 for SW winds: (a) wind speed, (b) turbulent kinetic energy (c) wind direction

https://doi.org/10.5194/wes-2021-142
Preprint. Discussion started: 20 January 2022

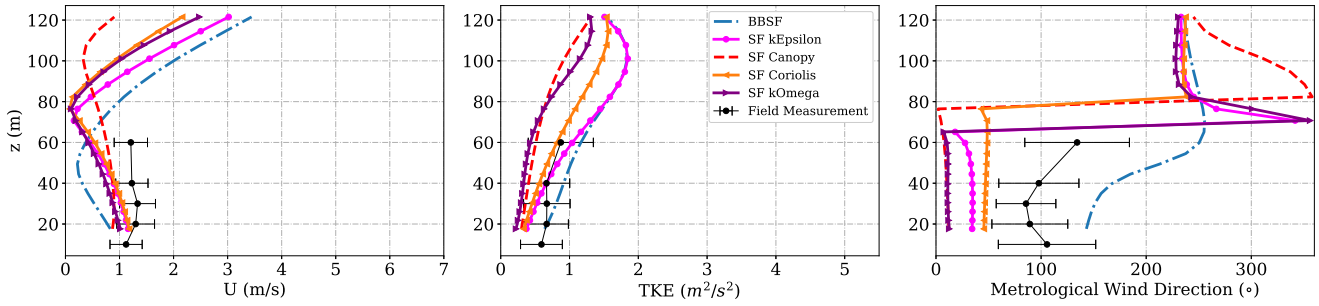

Figure 12. Simulation results and experimental data in tower 22/ tse06 for SW winds: (a) wind speed, (b) turbulent kinetic energy (c) wind direction

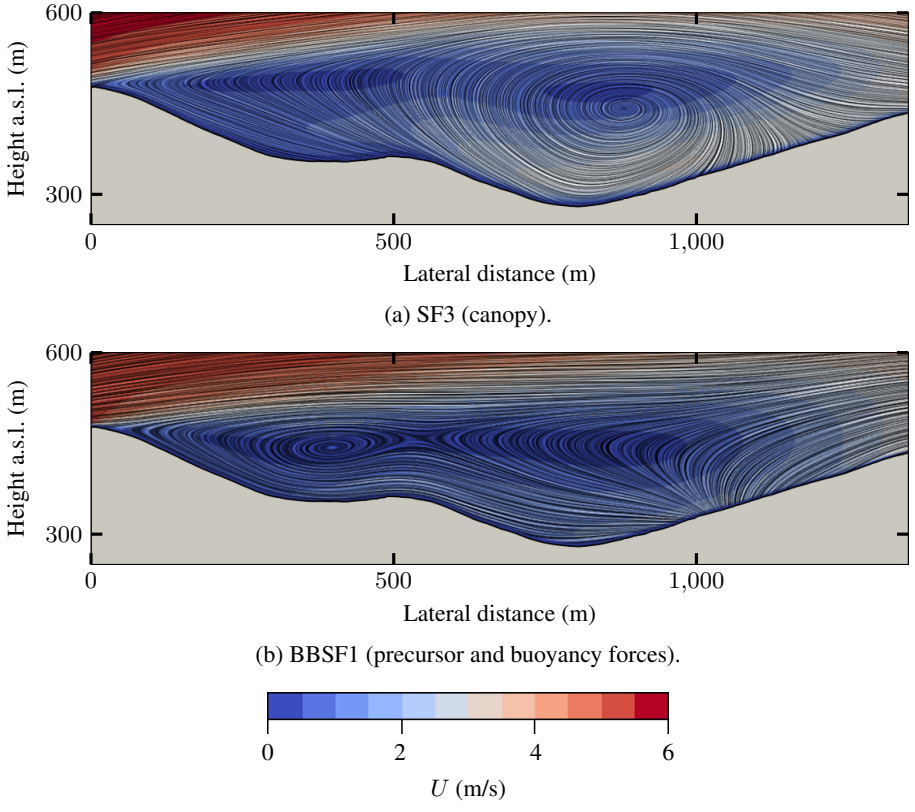

Figure 13. Re-circulation zone inside the valley. Slice of velocity magnitude, U, and flow patterns.

https://doi.org/10.5194/wes-2021-142
Preprint. Discussion started: 20 January 2022

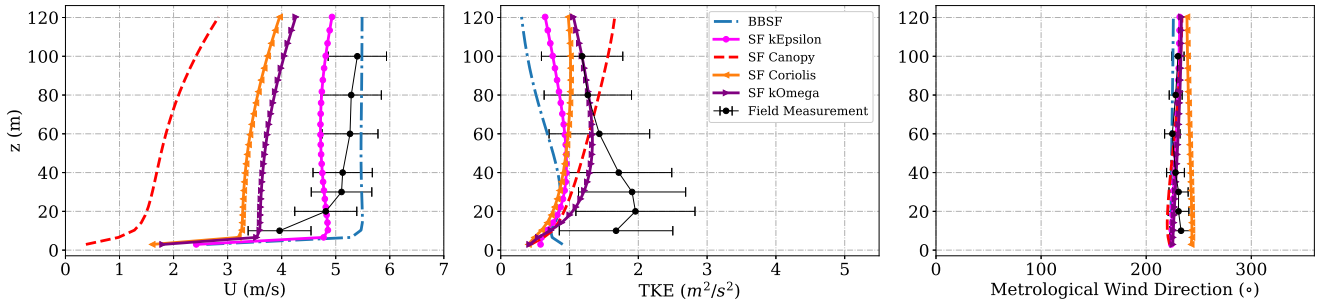

Figure 14. Simulation results and experimental data in tower 29/ tse13 for SW winds: (a) wind speed, (b) turbulent kinetic energy (c) wind direction

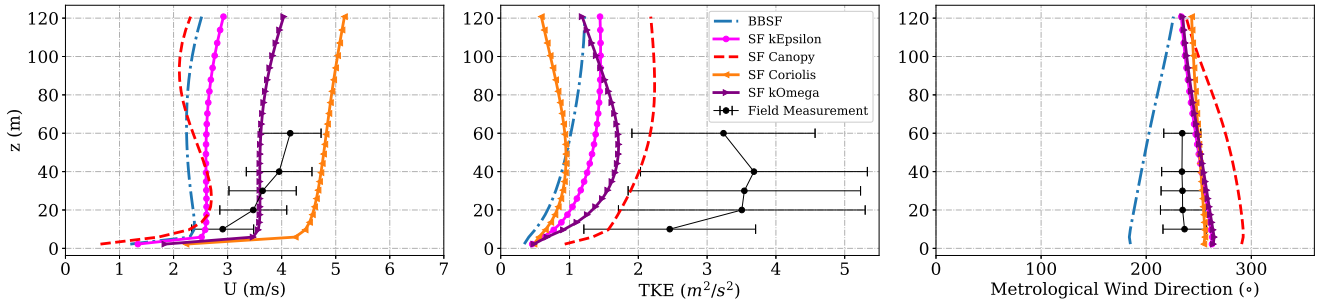

Figure 15. Simulation results and experimental data in tower 10/ tnw10 for SW winds: (a) wind speed, (b) turbulent kinetic energy (c) wind direction

4.3 Tower Prediction on NE ridge

The predictions for towers on the North-East ridge Tower 29 and Tower 10 are shown in Figs. 14 and 15. This is a region of flow acceleration on top of the ridge downstream from re-circulation zone inside the valley, which makes the predictions quite challenging. The canopy model is seen to under predict significantly the velocity profiles on top of this ridge. Both the baseline $k-\epsilon$ model and buyoantBoussinesqSimpleFoam model appears to provide a good prediction of the velocity profile and wind direction for the Tower 29 and also Tower 10 upto 40 m. The region near tower 10 comprises of a mountain gap (Vassallo et al. 2020), which could indicate that a higher terrain resolution is required surrounding this region to improve the prediction accuracy.

https://doi.org/10.5194/wes-2021-142
Preprint. Discussion started: 20 January 2022

eawe european academy of wind energy
Open Access WIND ENERGY SCIENCE DISCUSSIONS

5 Conclusions

A Reynolds-averaged Navier-Stokes (RANS) model is setup using OpenFOAM (version 2012) to simulate a 30 min averaged period corresponding to a neutral atmospheric stability condition at Tower 20. The predicted profiles are analysed in terms of the different groups of towers on top of the ridges and inside the valley based on the flow topology. Five different models are simulated comprising of different source terms to take into account the effects of buoyancy, canopy, Coriolis forces. The complex terrain site of Perdigão represents a large spatial variability of forest canopy and surface elevation, which contribute to variable thermal stability at different met-masts. The key conclusions for different groups of towers are summarised as follows:

a) **For the towers on the South-West ridge:** The region at the South-West ridge is a zone flow acceleration upstream of the inflow wind direction. The use of canopy model decreases the velocities near the surface and a closer match with field data. Other models over-predict the velocity profile close to the ground. However, the canopy parameters need to be tuned as the surface heterogeneity is not taken into account as the prediction accuracy varies at the different locations along the ridge.

b) **For the towers inside the valley:** The valley is a zone of flow re-circulation. and comprises lower velocities and higher variability which remains challenging for prediction models. The BBSF model is shown to provide the best prediction of wind direction. Large relative errors in wind speed and turbulent kinetic energy profiles are seen for most of the models.

c) **For the towers on the North-East ridge**: The region at the North-East ridge is a zone of flow acceleration downstream of the re-circulation zone from the valley. Significant turbulence is seen close to ground in the field measurements, which is under-predicted by most of the models. The model accounting for buoyancy forces provides a good prediction on Tower 29 for the wind speed and direction while the canopy model strongly under predicts the wind speed. Local terrain features need to be resolved such as the mountain gap near Tower 10.

Finally, the choice of the best turbulence model is found to be inconclusive in terms of overall prediction capability for different parts of the terrain. In the future, the surface heterogeneity of canopy is to be modelled based on the surface roughness map at Perdigão. The inclusion of the canopy model in buoyantBoussinesq solver could help evaluate the benefit of incorporating both canopy and buoyancy effects together. Furthermore, simulations shall be performed for periods of non-neutral flow conditions, such as stable or unstable thermal stratification conditions, where the buoyancy effects play an important role.

Acknowledgements. The authors acknowledge the European Commission for its financial support through the project H2020-MSCA-ITN-2019 zEPHYR (Grant Agreement No. 860101). Perdigao data provided by NCAR/EOL under the sponsorship of the National Science Foundation. https://data.eol.ucar.edu/

https://doi.org/10.5194/wes-2021-142
Preprint. Discussion started: 20 January 2022

eawe european academy of wind energy
Open Access WIND ENERGY SCIENCE DISCUSSIONS

Author contributions: KV conceived, coordinated and was responsible for both the work and the manuscript writing. TOH carried out the numerical simulations, manuscript writing and preparation of figures. SB helped with conception, manuscript writing and review. KEG helped with model setup and review.

Competing interests: The authors declare that they have no conflict of interest.

https://doi.org/10.5194/wes-2021-142
Preprint. Discussion started: 20 January 2022

eawe european academy of wind energy
Open Access WIND ENERGY SCIENCE DISCUSSIONS

References

Alletto, M., Radi, A., Adib, J., Langner, J., Peralta, C., Altmikus, A., and Letzel, M. (2018). E-wind: Steady state cfd approach for stratified flows used for site assessment at enercon. *Journal of Physics: Conference Series*, 1037:072020.

Bechmann, A., Berg, J., Courtney, M., Jørgensen, H., Mann, J., and Sørensen, N. (2009). The bolund experiment: Blind comparison of models for wind in complex terrain (invited). *AGU Fall Meeting Abstracts*.

Blackadar, A. K. (1962). The Vertical Distribution of Wind and Turbulent Exchange in a Neutral Atmosphere. *Journal of Geophysical Research*, 67(3):3095.

Blocken, B. (2014). 50 years of computational wind engineering: Past, present and future. *Journal of Wind Engineering and Industrial Aerodynamics*, 129:69–102.

Brower, M. (2012). Findings of investigations into under-performing sites. In *Proceedings of EWEA Technology Workshop, Lyon, France.* European Wind Energy Association (EWEA).

Carvalho, J. P. D. B. (2019). Analysis of stationary periods during the Perdigao 2017 campaign. Master's thesis, University of Porto, Portugal.

Chavez, R., Rodrigo, J., and Gancarski, P. (2014). Modelling of atmospheric boundary-layer flow in complex terrain with different forest parameterizations. volume 524.

Costa, J. L. C. (2007). Atmospheric flow over forested and non-forested complex terrain.

Desmond, C., Watson, S., and Hancock, P. (2017). Modelling the wind energy resources in complex terrain and atmospheres. numerical simulation and wind tunnel investigation of non-neutral forest canopy flows. *Journal of Wind Engineering and Industrial Aerodynamics*, 166:48–60.

Emeis, S. (2018). *Wind Energy Meteorology*, volume 2 of *Atmospheric Physics for Wind Power Generation*. Springer International Publishing, Belgium.

Fernando, H., Mann, J., Laginha Palma, J., Lundquist, J., Barthelmie, R., Belo-Pereira, M., Brown, W., Chow, F., Gerz, T., Hocut, C., Klein, P., Leo, L., Matos, J., Oncley, S., Pryor, S., Bariteau, L., Bell, T., Bodini, N., Carney, M., and Wang, Y. (2018). The perdigão: Peering into microscale details of mountain winds. *Bulletin of the American Meteorological Society*, 100.

Finnigan, J. (2000). Turbulence in plant canopies. ann rev fluid mech. *Annual Review of Fluid Mechanics*, 32:519–571.

Hågbo, T.-O., Giljarhus, K. E. T., and Hjertager, B. H. (2020). Influence of geometry acquisition method on pedestrian wind simulations. *arXiv preprint arXiv:2010.12371*.

Hargreaves, D. and Wright, N. G. (2007). On the use of the k–ε model in commercial cfd software to model the neutral atmospheric boundary layer. *Journal of wind engineering and industrial aerodynamics*, 95(5):355–369.

Jørgensen, H., Nielsen, M., Barthelmie, R., and Mortensen, N. (2005). Modelling offshore wind resources and wind conditions. *In Proceedings (CD-ROM) Copenhagen Offshore Wind.*

Kaimal, J. C. and Finnigan, J. J. (1994). *Atmospheric boundary layer flows: Their structure and measurement*. Oxford University Press.

Koblitz, T. (2013). *CFD Modeling of Non-Neutral Atmospheric Boundary Layer Conditions*. PhD thesis, Denmark.

Laginha Palma, J., Silva, C., Costa Gomes, V., Lopes, A., Esteves, T., and Batista, V. (2020). The digital terrain model in the computational modelling of the flow over the perdigão site: the appropriate grid size. *Wind Energy Science*, 5:1469–1485.

OpenFOAM. Openfoam v2012. https://www.openfoam.com/documentation/overview. Accessed: 2021-08-21.

Queck, R., Bienert, A., Maas, H.-G., Harmansa, S., Goldberg, V., and Bernhofer, C. (2012). Wind fields in heterogeneous conifer canopies: Parameterisation of momentum absorption using high-resolution 3d vegetation scans. *European Journal of Forest Research*, 131:165–176.

https://doi.org/10.5194/wes-2021-142
Preprint. Discussion started: 20 January 2022

Richards, P. and Hoaxey, R. (1993). Appropriate boundary conditions for computational wind engineering models using the k-ϵ turbulence model. In Murakami, S., editor, *Computational Wind Engineering 1*, pages 145–153. Elsevier, Oxford.

Rodrigo, J., Santos, P., Chavez, R., Avila, M., Cavar, D., Lehmkuhl, O., Owen, H., Li, R., and Tromeur, E. (2021). The alex17 diurnal cycles in complex terrain benchmark. *Journal of Physics: Conference Series*, 1934:012002.

Salmon, J., Bowen, A., Hoff, A., Johnson, R., Mickle, R., Taylor, P., Tetzlaff, G., and Walmsley, J. (1988). The askervein hill project: Mean wind variations at fixed heights above ground. *Boundary-Layer Meteorology*, 43:247–271.

Schmidt, J., Peralta, C., and Stoevesandt, B. (2012). Automated generation of structured meshes for wind energy applications. Open Source CFD International Conference, London.

Sogachev, A. (2009). A note on two-equation closure modelling of canopy flow. *Boundary-Layer Meteorology*, 130:423–435.

Sogachev, A. and Panfyorov, O. (2006). Modification of two-equation models to account for plant drag. *Boundary-Layer Meteorology*, 121:229–266.

Sørensen, N. N., Bechmann, A., Réthoré, P.-E., Cavar, D., Kelly, M. C., and Troen, I. (2012). How fine is fine enough when doing CFD terrain simulations. In *EWEA 2012-European Wind Energy Conference & Exhibition*, pages 1167–1172. European Wind Energy Association (EWEA).

Temel, O., Bricteux, L., and Beeck, J. (2018). Coupled wrf-openfoam study of wind flow over complex terrain. *Journal of Wind Engineering and Industrial Aerodynamics*, 174:152–169.

van der Laan, M. P., Kelly, M., Floors, R., and Peña, A. (2020). Rossby number similarity of an atmospheric rans model using limited-length-scale turbulence closures extended to unstable stratification. *Wind Energy Science*, 5:355–374.

Vasiljevic, N., Laginha Palma, J., Angelou, N., Matos, J., Menke, R., Lea, G., Mann, J., Courtney, M., Frölén Ribeiro, L., and Costa Gomes, V. (2017). Perdigão 2015: methodology for atmospheric multi-doppler lidar experiments. *Atmospheric Measurement Techniques Discussions*, pages 1–28.

Vassallo, D., Krishnamurthy, R., Menke, R., and Fernando, H. (2020). Observations of stably stratified flow through a microscale gap. *Journal of the Atmospheric Sciences*, 78.

Wagner, J., Wildmann, N., and Gerz, T. (2019). Improving boundary layer flow simulations over complex terrain by applying a forest parameterization in WRF. *Wind Energ. Sci. Discuss. [preprint]*.

Yang, Y., Gu, M., Chen, S., and Jin, X. (2009). New inflow boundary conditions for modelling the neutral equilibrium atmospheric boundary layer in computational wind engineering. *Journal of Wind Engineering and Industrial Aerodynamics*, 97(2):88–95.